

# Characteristics of the finite Olver Gaussian beam propagating in the sandwich slab system

LONG JIN\*, XINGQIANG ZHANG

*Department of Basic Science, Hubei University of Automotive Technology, 167 Checheng West Road, Shiyan City 442002, Hubei province, China*

---

Based on the transfer matrix and generalized Huygens-Fresnel integral equation, the evolution of a finite Olver Gaussian beam (FOGB) propagating in the multilayered sandwich slab system contained right handed material and double negative material alternate is studied in detail, the influence of adjustment factor and decay factor on the FOGB intensity evolution is further researched, the transmission properties of finite Airy Gaussian beam (FAiGB) regarded as the zeroth-order non-diffracting beam of the FOGB is discussed as well. In addition, we also propose an optical sensor to measure the concentration of alcohol solution, of which the operating principle is thoroughly explored. It is expected that the proposed optical sensor and the corresponding conclusions will be a useful supplement to chemical concentration detector.

(Received January 31, 2018; accepted April 8, 2019)

*Keywords:* Physical optics, Finite Olver Gaussian beam, Transfer matrix, Generalized Huygens-Fresnel integral equation, Double negative material, Optical sensor

---

## 1. Introduction

Ever since Veselago first theoretically reported the dielectric media with both negative permittivity  $\epsilon$  and negative permeability  $\mu$  in 1968 [1], debates on the metamaterials so-called double negative materials (DNM) have almost never stopped [2-3]. In 2001, Smith *et al.* creatively used the copper to produce the artificial DNM, for the first time, in microwave [4]. From then on, the multilayered structures [5-6], such as photonic crystal, optical film, contained DNM have been investigated theoretically and experimentally since DNM have many dramatically unprecedented phenomena compared with right handed materials (RHM), for instance, beam focusing and phase compensation, large negative lateral shift, negative refraction EM energy, inverse Cerenkov radiation, reverse Doppler effect, negative reverse pressure, etc. [7].

On the other hand, in 1979, Berry and Balazs proved for the first time that Airy function was an exact solution of Schrodinger equation in the context of quantum mechanics [8]. However, this predicted Airy beam carries infinite energy and not realizable physically. To overcome the defect mentioned above, the finite Airy beam (FAiB), which also have unique properties such as self-healing, self-acceleration, self-bending and non-diffraction, was first studied both theoretically and experimentally by Siviloglou *et al.* in 2007 [9-10]. Recently, diffraction free beam families have been revolutionized once again, the Finite Olver beam (FOB) introduced by Belafhal *et al.* is demonstrated as a newborn non-diffracting beam, and regarded as a

generalization of the well-known FAiB [11]. Since then, a great deal of attention has been paid to this novel beam propagation characteristic, transmission of the FOB passing through a paraxial optical system [12], a misaligned optical system, including rectangle aperture and annular aperture [13-14], a right handed and double negative index slab system [15], and the uniaxial crystal [16] have been reported. To date, as far as we know, the propagation properties of the Finite Olver Gaussian beam (FOGB) passing through the multilayered structures contained RHM and DNM alternate has not been studied elsewhere, the Gaussian beam and the correlation techniques are still an important research topic in laser optics.

In this letter, we particularly focus on the FOGB intensity profiles on output cross section, and the side view of this beam propagating in a sandwich slab system. The rest of the paper is organized as follows: in section 2, the analytical expression of the FOGB passing through the paraxial optical system is calculated in the space domain by the transfer matrix and generalized Huygens-Fresnel integral equation. In section 3, the emerging beam intensity and side view when the FOGB propagates in the sandwich slab system are discussed in detail, we mainly focus on the influences of the adjustment factor, the decay factor, and the negative index parameters on the FOGB intensity evolution. Furthermore, a numerical example of engineering application is given in section 4: we propose an optical sensor to measure the concentration of alcohol solution. Finally, section 5 summarizes the main results obtained in this paper.

## 2. Optical model and theoretical analysis

Within the frame of Cartesian coordinates, we set the  $z$  axis as the beam propagation direction, a three-dimensional slab system is constituted of RHM and DNM alternately with its leftmost texture locating at  $z=0$ , the medium unit with black colour signifies RHM and the blue denotes DNM, as depicted in Fig. 1, it is a type of periodic structure more like the ‘sandwich’. Here, we select the lossless isotropic DNM with its relative permittivity and permeability given by the Drude characteristics [17]

$$\varepsilon_r(\omega) = 1 - \frac{\omega_{pe}^2}{\omega^2} \quad (1)$$

$$\mu_r(\omega) = 1 - \frac{\omega_{pm}^2}{\omega^2} \quad (2)$$

where  $\omega_{pe}$  and  $\omega_{pm}$  are the electric plasma frequency and the magnetic plasma frequency, respectively,  $\omega$  is the angular frequency of the input wave, the length of each DNM unit is  $L$ , and the frequency dependent refractive index for each DNM unit reads as

$$n_l = -\sqrt{\varepsilon_r(\omega) \cdot \mu_r(\omega)} \quad (3)$$

In terms of RHM, its refractive index and the unit length are  $n_r$  and  $R$ , respectively.

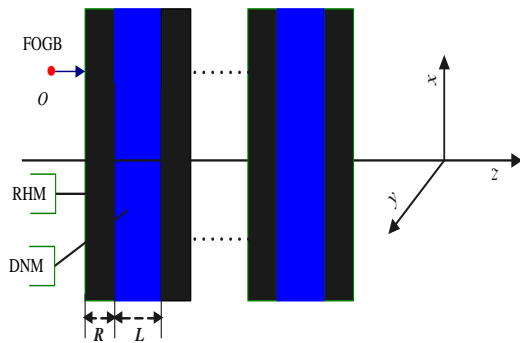


Fig. 1. Schematic diagram of the FOGB passing through the sandwich slab system

The electric field distribution of the input FOGB at the initial plane  $z=0$  (point  $O$ ) can be described as

$$E_1(x_0, y_0) = \exp\left(\frac{a_0 x_0}{\omega_1} + \frac{a_0 y_0}{\omega_2}\right) \times \exp\left(-\frac{x_0^2 + y_0^2}{\omega_0}\right) O_n\left(\frac{x_0}{\omega_1}\right) O_n\left(\frac{y_0}{\omega_2}\right) \quad (4)$$

with  $0 \leq a_0 < 1$  denotes the decay factor,  $\omega_1$  and  $\omega_2$  signify the arbitrary transverse scales in the  $x$  and  $y$  directions, and  $\omega_1 = \omega_2 = \zeta \omega_0$ , where  $\omega_0$  is beam waist size, and  $\zeta$  is the adjustment factor.  $O_n(\bullet)$  is the  $n$ -th order Olver function with  $n$  being the order of Olver function, or the order of the beam in the framework of physical optics, and the integral equation of  $O_n(\bullet)$  is defined by the following expression

$$O_n(x) = \frac{1}{2\pi} \times \int_{-\infty}^{+\infty} e^{ix} \text{pd} [i(\zeta u + i) - i u x] \quad (5)$$

where

$$\begin{cases} \gamma = n + 3, \\ |a| = \frac{1}{n + 3}. \end{cases} \quad (6)$$

One can find out that the Olver function will reduce to the ordinary Airy function in the event of  $n=0$ , under this circumstance, the incident beam also degrades into a finite Airy-Gaussian one (FAiGB).

The propagation of the FOGB passing through the paraxial optical system, calculated by the transfer matrix, follows the principle of the generalized Huygens-Fresnel integral equation [12-14]

$$E_2(x, y, z) = \left(\frac{-i}{\lambda B}\right) e^{ikz} \iint_{s_1} E_1(x_0, y_0) e^{\frac{ik}{2B}[A(x_0^2 + y_0^2) + D(x^2 + y^2) - 2(xx_0 + yy_0)]} dx_0 dy_0 \quad (7)$$

with  $\lambda=1.55 \mu\text{m}$  is the input wave length,  $k=2\pi/\lambda$  is the wave number.  $A$ ,  $B$ ,  $C$  and  $D$  are the transfer matrix elements of the total paraxial optical systems, as to our sandwich model, the total transfer matrix  $T$  reads [18-19]

$$T = \begin{pmatrix} A & B \\ C & D \end{pmatrix} = [M(n_r, 1) \times M(R) \times M(n_l, n_r) \times M(L) \times M(n_r, n_l) \times M(R) \times M(1, n_r)]^m \quad (8)$$

where

$$M(l) = \begin{pmatrix} 1 & l \\ 0 & 1 \end{pmatrix} \quad (9)$$

with  $l=L$  or  $R$  expresses the beam propagates a distance  $l$  in the heterogeneous medium. When the beam propagates from RHM into DNM unit, the transfer matrix form in RHM-DNM interface is described as

$$M(n_r, n_l) = \begin{pmatrix} 1 & 0 \\ 0 & \frac{n_r}{n_l} \end{pmatrix} \quad (10)$$

In the same way, DNM-RHM interface transfer matrix denotes

$$M(n_l, n_r) = \begin{pmatrix} 1 & 0 \\ 0 & \frac{n_l}{n_r} \end{pmatrix} \quad (11)$$

$m$  is period number of this system, here we set up the parameter  $m=1$  in order to facilitate the simulation. By cross-producing these transfer matrices in accordance with the order of the beam propagating from air to the sandwich slab, we can acquire the specific values of the total transfer matrix

$$T = \begin{pmatrix} 1 & \left( R + \frac{n_r \times (L + \frac{n_l \times R}{n_r})}{n_l} \right) / n_r \\ 0 & 1 \end{pmatrix} \quad (12)$$

Substituting Eq. (12) into Eq. (7), the electric field of the output FOGB passing through the paraxial  $ABCD$  optical system in space domain is expressed as

$$E_2(x, y, z) = \frac{ik}{2BM} \times \exp(h(x, y, z)) \times O_n(p(x))O_n(q(y)) \quad (13)$$

where

$$h(x, y, z) = -\frac{ik}{2B}(x^2 + y^2) - \frac{k^2}{4B^2M}(x^2 + y^2) + \frac{ik}{8BM^2} \left( \frac{x}{\omega_1^3} + \frac{y}{\omega_2^3} \right) + \frac{ika_0}{2BM} \left( \frac{x}{\omega_1} + \frac{y}{\omega_2} \right) + \frac{1}{96M^3} \left( \frac{1}{\omega_1^6} + \frac{1}{\omega_2^6} \right) + \frac{a_0}{8M^2} \left( \frac{1}{\omega_1^4} + \frac{1}{\omega_2^4} \right) + \frac{a_0^2}{4M} \left( \frac{1}{\omega_1^2} + \frac{1}{\omega_2^2} \right) \quad (14)$$

$$p(x) = \frac{ikx}{2BM\omega_1} + \frac{a_0}{2M\omega_1^2} + \frac{1}{16M^2\omega_1^4} \quad (15)$$

$$q(y) = \frac{iky}{2BM\omega_2} + \frac{a_0}{2M\omega_2^2} + \frac{1}{16M^2\omega_2^4} \quad (16)$$

$$M = \frac{1}{\omega_0} + \frac{ik}{2B} \quad (17)$$

$x$  and  $y$  represent two paraxial transverse coordinates in any paraxial cross section. The light intensity is gained by using the complex conjugate of  $E(x, y, z)$

$$I = \frac{n}{2c\mu_0} |E(x, y, z)|^2 \propto |E(x, y, z)|^2, \quad (18)$$

where  $c$  and  $\mu_0$  are the speed of light and permeability in the vacuum.

### 3. Numerical simulation and analysis

#### 3.1. Intensity distribution of the FOGB passing through the sandwich slab system

As numerical examples, we start with discussing the intensity distribution of the output FOGB and the side view of this beam propagates in the sandwich slab system, where  $a_0=0$ ,  $\omega_0=0.01\text{m}$ ,  $\zeta=0.07$ , and  $n=2$ , the relative permittivity and permeability parameters are set as  $\omega_{pe}=\omega_{pm}=2\pi\nu\times\sqrt{2.5}$ , where  $\nu=c/\lambda=1.94\times 10^{14}\text{Hz}$ , leading to the corresponding refractive indexes  $n_l=-1.5$ ,  $n_r=1.5$  fixed, the Rayleigh distance of this beam is  $Z_R=k\omega^2/2$ , and  $R=10Z_R$ ,  $L=20Z_R$ . For comparing and analyzing the influence of beam order  $n$  on the wave intensity evolution, the well-known FAiGB regarded as the zeroth-order non-diffracting FOGB is also demonstrated in Fig. 2. It is discovered that the self-bending FOGB experiences negative refraction in the middle DNM and goes back to its original outline when passes through the whole slab, as shown in Fig. 2(a), Pendry once illuminated that the middle DNM is like a perfect lens, which enables the output planar wave to reconstruct and come back to its original feature [20], this theory is also suitable for the FOGB propagating in the multilayer slab system contained DNM. By contrasting Fig 2(b) and Fig. 2(a), we obtain that the emerging FAiGB has much more side lobes, but the smaller main lobe spot size, than the emerging FOGB under the condition that other parameters are the same. Furthermore, the basic characteristics of the FAiGB in our simulation agree with the article published by Gutiérrezvega *et al.* [21].

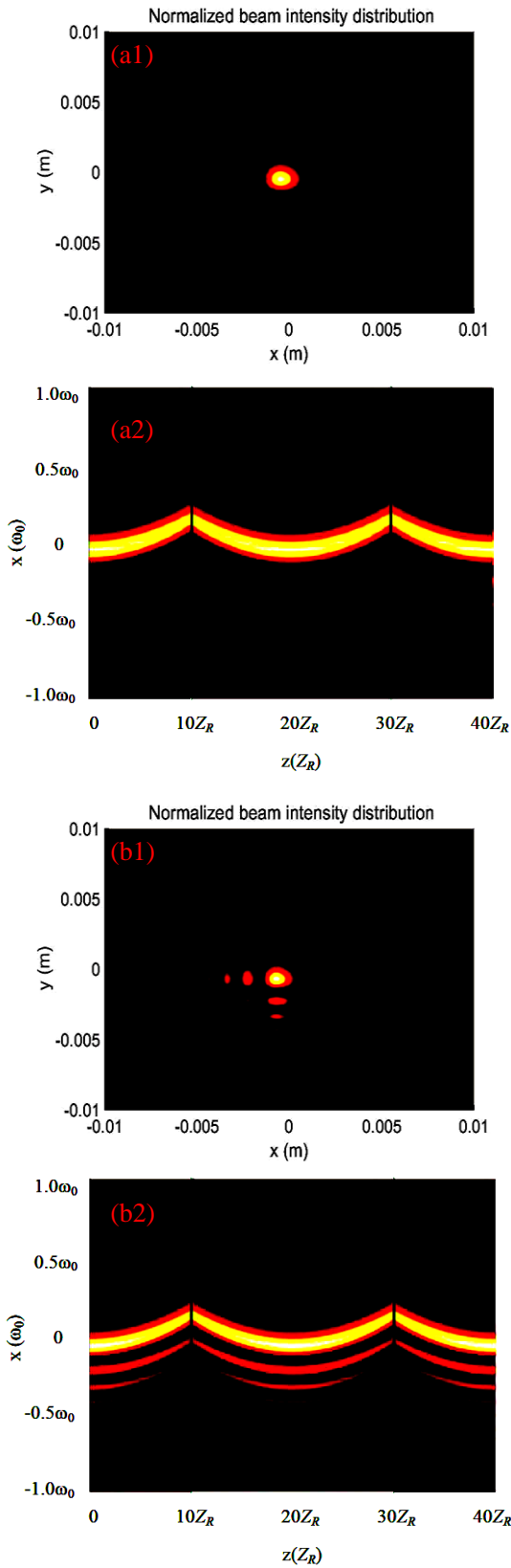


Fig. 2. Intensity distribution of the FOGB propagates in the sandwich slab system. (a1) Output beam intensity distribution,  $n=2$ ; (a2) Beam side transmission view,  $n=2$ ; (b1) Output beam intensity distribution,  $n=0$ ; (b2) Beam side transmission view,  $n=0$

### 3.2. Emerging beam intensity distribution changed with the adjustment factor

Now, we delve into the emerging FOGB intensity distribution changed with the adjustment factor  $\zeta$ , the numeric result is depicted in Fig. 3, the other parameters are the same as those in Fig. 2 except  $\zeta=0.05$  and 0.1, respectively. By viewing Fig. 3 (a), (b) and Fig. 2(a1), it is come to the conclusion that the fundamental characteristics of the FOGB are not affected by the increasing of the adjustment factor  $\zeta$ , merely the larger the  $\zeta$  is, and the bigger the lobes spot size is formed.

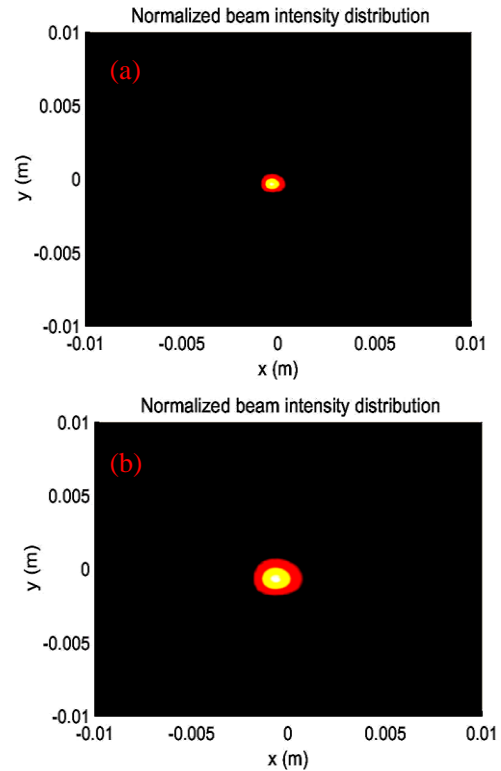


Fig. 3. Output intensity distribution of the FOGB changed with different adjustment factor  $\zeta$ . (a)  $\zeta=0.05$ ; (b)  $\zeta=0.1$

### 3.3. Influence of decay factor on emerging beam intensity distribution

To explore how the decay factor  $a_0$  acts on the emerging FOGB intensity distribution, figure 4 describes its output intensity changed with  $a_0=0.1$  and 0.5, the other parameters are the same as those in Fig. 2. We can acquire from these figures that the number of side lobes decreases with the increasing of decay factor  $a_0$ , while  $a_0=0$  in Fig. 2(a1), lots of side lobes gather around  $-x$  axis,  $-y$  axis and the third quadrant, however, only the main lobe exists when  $a_0=0.5$ , as shown in Fig. 4 (b), hence, we conclude that the decay factor  $a_0$  can control the beam's outline that more like a finite Olver beam

with a smaller value, and a finite Gaussian beam with a larger one, which is very useful for extension applications of optical control.

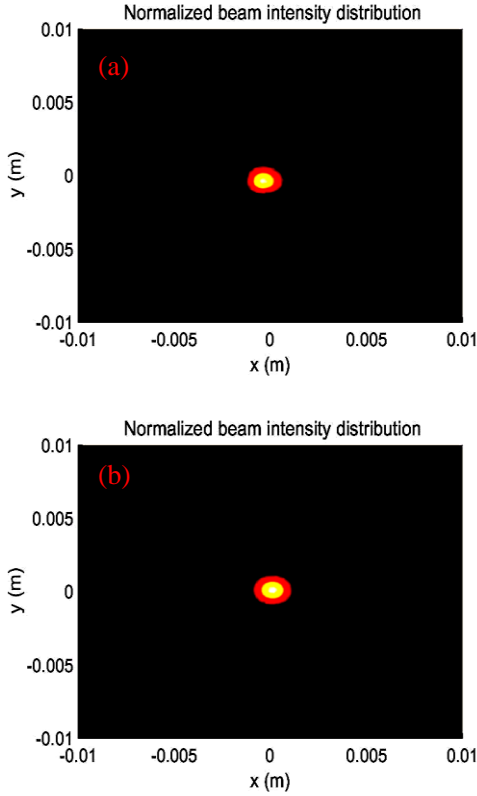


Fig. 4. Influence of decay factor  $a_0$  on the output FOGB intensity distribution. (a)  $a_0=0.1$ ; (b)  $a_0=0.5$

### 3.4. Influence of negative index parameters on beam evolution

In this subsection, we discuss the FOGB intensity evolution with different negative index parameters, the emerging beam intensity and beam side view are demonstrated in Fig. 5, where  $a_0=0.5$ ,  $\zeta=0.1$ , we choose  $\omega_{pe}=\omega_{pm}=2\pi\nu\times\sqrt{2.0}$  and  $\omega_{pe}=\omega_{pm}=2\pi\nu\times\sqrt{3.0}$ , which result in the corresponding refractive indexes  $n_l=-1.0$ , and  $-2.0$ , respectively, the other parameters are the same as those in Fig. 2. It is easily observed from Fig. 5 (a2) and (b2) that the output beam cannot come back to its original feature if the negative index parameter  $\text{abs}(n_l) \neq n_r=1.5$ . While  $\text{abs}(n_l) < n_r$  in Fig. 5 (a), the output beam converges at the end of the RHM unit, otherwise, the emerging beam diverges and self-bends again. By using this method, we can regulate the FOGB evolution process by changing different DNM unit.

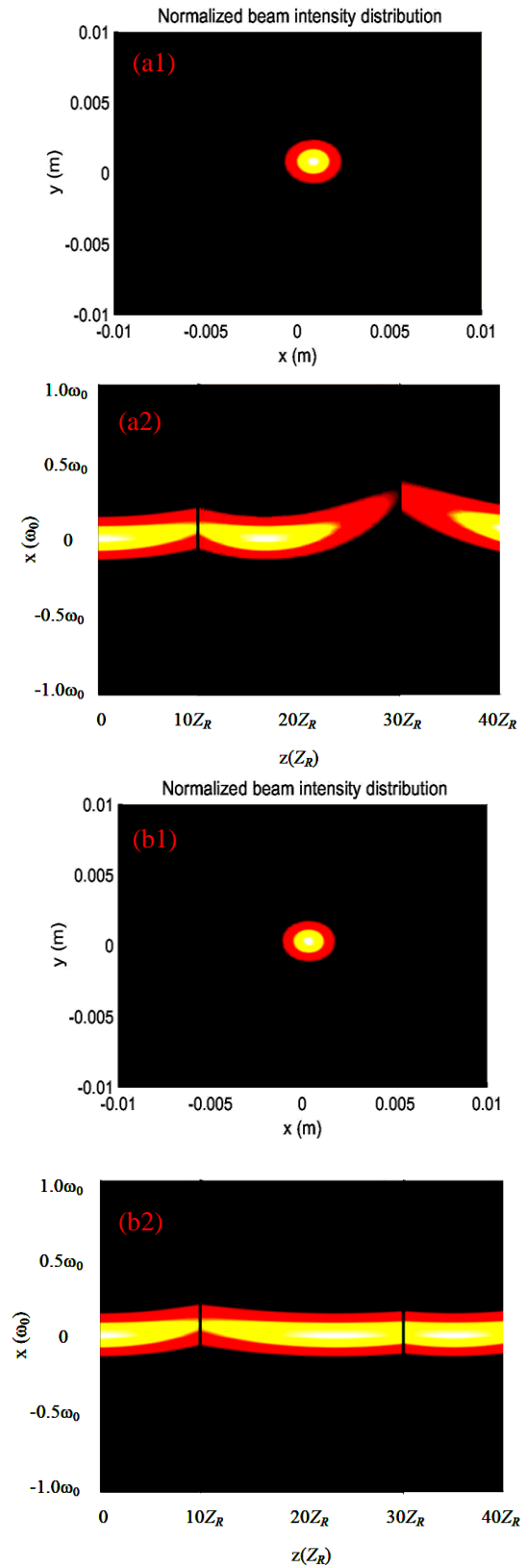


Fig. 5. Influence of negative index parameter  $n_l$  on beam intensity evolution. (a1) Output beam intensity distribution,  $n_l=-1.0$ ; (a2) Beam side transmission view,  $n_l=-1.0$ ; (b1) Output beam intensity distribution,  $n_l=-2.0$ ; (b2) Beam side transmission view,  $n_l=-2.0$

#### 4. Engineering application

RHM can affect the evolution of the FOGB as well as DNM, of which the regulation principle is similar to those represented in above section 3.4, and based on that, we propose an optical sensor to measure the concentration of alcohol solution. The design concept of this sensor is: each RHM is substituted by alcohol solution concentration, and the middle DNM  $n_i=-1.5$  maintains unchanged, the other parameters are the same as those in Fig. 5. When beam passes through this sandwich slab system filled with different concentration of alcohol solution, the beam intensity distribution and maximum intensity value on output cross section vary with the alcohol solution concentration. A contrast is made between two kinds of beam intensity, purified water and 90% alcohol solution's, is demonstrated in Fig. 6, it is apparent from the colour bar that the higher the alcohol concentration is, the stronger the maximum intensity is formed on output cross section.

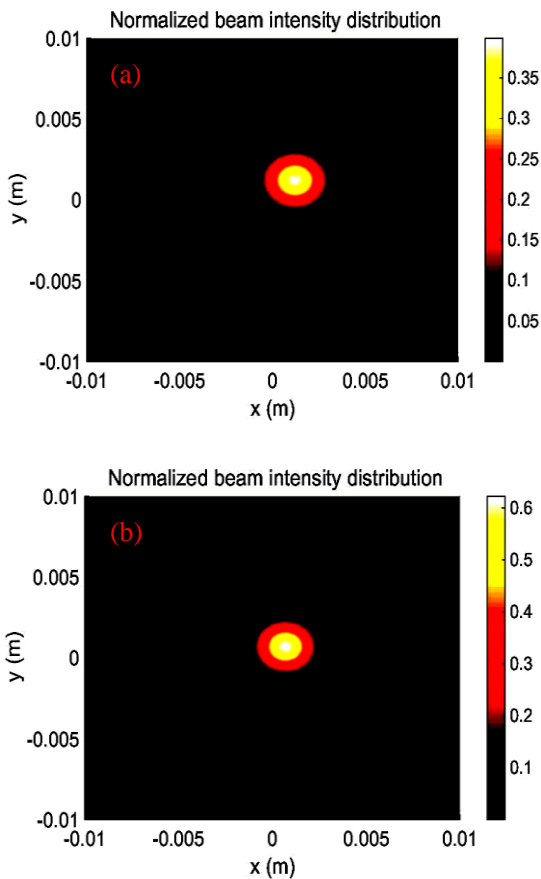


Fig. 6. Output intensity distribution of the FOGB changed with different concentration of alcohol solution. (a) Intensity distribution to purified water; (b) Intensity distribution to 90% alcohol solution

In order to better understanding the operating principle of this optical sensor, quantitative research between beam normalized maximum intensity and

alcohol concentration is expanded as follow. The empirical formula between alcohol solution concentration and its refractive index is given by [22]

$$\delta = 1.33456 + 4.6726 \times 10^{-4} N \quad (19)$$

where  $N$  is refractive index and  $\delta$  is alcohol solution concentration. Substituting Eq. (19) into Eq. (12), we obtain the relation between alcohol solution concentration  $\delta$  and the transfer matrix element  $B$  as following

$$B = \frac{\left(\frac{2L}{3} + \frac{a_2 R}{a_1 - \delta}\right) \times (a_1 - \delta) - a_2 \left(R + \frac{a_2}{a_1 - \delta}\right)}{a_1 - \delta} \quad (20)$$

where  $a_1=1.33456$ ,  $a_2=4.6726 \times 10^{-4}$ . When the alcohol solution abound in each RHM unit, the relation between the emerging normalized maximum intensity and the solution refractive index, the solution concentration are demonstrated in Fig. 7 and Fig. 8, respectively. It is clearly observed that both curves are in possession of good linear properties. The mathematical formula corresponding to Fig. 8 is acquired by linear fitting method, and the ultimatum is

$$I = 0.38683 + 0.00248 \times \delta \quad (21)$$

where  $I$  signifies the normalized maximum intensity. In addition, what we want to emphasize is that this optical sensor can detect other solution like sucrose and starch solution so long as correlation coefficients in Eq. (21) are adjusted. It is expected that the optical sensor and corresponding conclusions can be useful for precise solution concentration measurement, such as food safety inspection and medical detection.

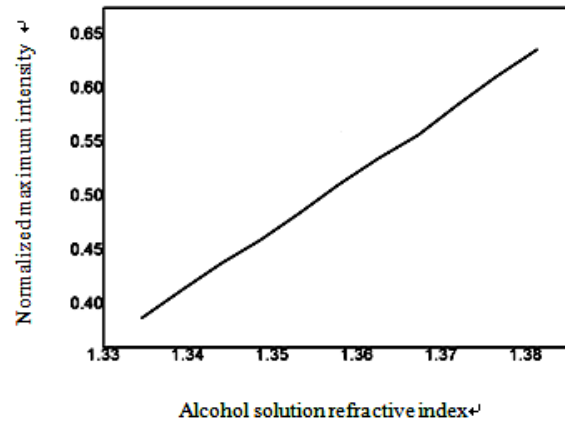


Fig. 7. Relation between normalized maximum intensity and alcohol solution refractive index

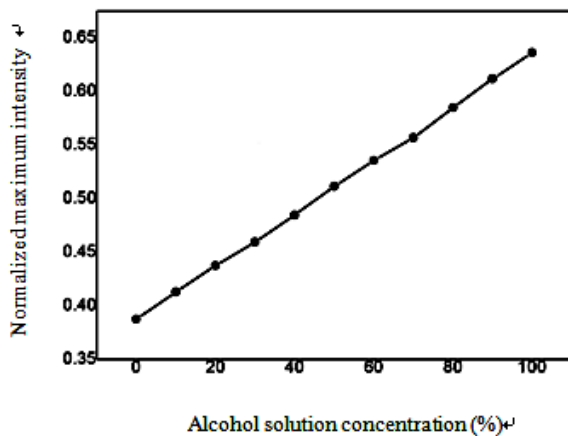


Fig. 8. Relation between normalized maximum intensity and alcohol solution concentration

## 5. Conclusion

In conclusion, we have delved into the evolution of the FOGB propagating in the sandwich slab system contained RHM and DNM alternate based on the transfer matrix and generalized Huygens-Fresnel integral equation, the transmission properties of FAiGB regarded as the zeroth-order non-diffracting beam of the FOGB is also researched. We have come to the conclusions that the output FOGB returns to its original feature when propagates the whole sandwich slab if  $n_l = -n_r$ , while  $\text{abs}(n_l) < n_r$ , the output beam converges at the end of the RHM unit, otherwise, the emerging beam diverges and self-bends again. The influence of same parameters on the FOGB intensity evolution has studied as well, we found that the fundamental characteristics of the output FOGB are not affected by the increasing the adjustment factor  $\zeta$ , merely the larger the  $\zeta$  is, the bigger the lobes spot size is, but the decay factor  $a_0$  can control the emerging beam outline that more like a finite Olver beam with a smaller value, and a finite Gaussian beam with a larger one. Meanwhile, we have proposed an optical sensor to measure the concentration of alcohol solution, of which the operating principle is thoroughly explored, the functional relation between normalized maximum intensity of the output FOGB and alcohol solution concentration is given by Eq. (21), we are sure that the proposed optical sensor and the corresponding conclusions will be a useful supplement to chemical concentration detector.

## Acknowledgements

The author wish to gratefully acknowledge enlightening discussion with engineer GUO Hong, who works at Dongfeng communications technology co. LTD, and the financial support from the Hubei Provincial Department of Education in china (No. B2017085). The authors would also like to thank the reviewers for their

comments which helped to improve this paper.

## References

- [1] V. G. Veselago, P. N. Lebedev, V. G. Veselago, Soviet Physics Uspekhi **10**(4), 509 (1968).
- [2] S. S. Islam, M. R. I. Faruque, M. T. Islam, Advanced Materials Research **974**(2), 33 (2014).
- [3] V. C. Henríquez, V. M. García-Chocano, Sánchez-Dehesa, J. Phys. Rev. Applied **8**(1), 014029 (2017).
- [4] R. A. Shelby, D. R. Smith, S. Schultz, Science **292**(5514), 77 (2001).
- [5] A. Aghajamali, A. Zare, C. J. Wu, Applied Optics **54**(29), 8602 (2015).
- [6] J. Li, T. Tang, L. Luo et al., Optics Express **25**(16), 19117 (2017).
- [7] V. G. Veselago, Applied Physics B **81**(2), 403 (2005).
- [8] M. V. Berry, N. L. Balazs, American Journal of Physics **47**(3), 264 (1979).
- [9] G. A. Siviloglou, J. Broky, A. Dogariu et al., Physical Review Letters **99**(21), 213901 (2007).
- [10] G. A. Siviloglou, D. N. Christodoulides, Optics Letters **32**(8), 979 (2007).
- [11] A. Belafhal, L. Ezzariy, S. Hennani et al., Optics & Photonics Journal **5**(7), 234 (2015).
- [12] S. Hennani, L. Ezzariy, A. Belafhal, Optics & Photonics Journal **5**(9), 273 (2015).
- [13] S. Hennani, L. Ezzariy, A. Belafhal, Optics & Photonics Journal **5**(12), 354 (2015).
- [14] S. Hennani, L. Ez-Zariy, A. Belafhal, Optik-International Journal for Light and Electron Optics, **136**, 573 (2017).
- [15] L. Jin, X. Zhang, Chinese Journal of Physics, **56**(3), 1105 (2018).
- [16] S. Hennani, L. Ez-Zariy, A. Belafhal, Progress in Electromagnetics Research M **45**, 153 (2016).
- [17] M. W. Feise, Y. S. Kivshar, Physics Letters A **334**(4), 326 (2005).
- [18] J. Zhou, H. Luo, S. Wen et al., Optics Communications **282**(14), 2670 (2009).
- [19] A. Ghatak, Optics, Beijing: Higher Education Press, **5**, 67 (2009).
- [20] J. Pendry, Physical Review Letters **85**(18), 3966 (2000).
- [21] J. C. Gutiérrezvega, M. A. Bandres, Optics Express **15**(25), 16719 (2007).
- [22] W. F. Zhou, S. G. Luo, C. K. Wang et al., Journal of Xingyi Normal University for Nationalities **5**(10), 119 (2013).

\*Corresponding author: crazyjinlong@163.com;  
20140007@huat.edu.cn